Performance-based emergency landing trajectory planning applying meta-heuristic and Dubins paths

Hassan Haghighi, Daniel Delahaye, Davood Asadi

Journal Pre-proof

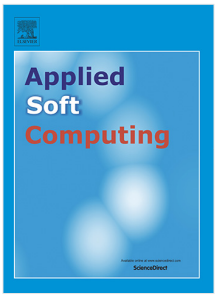

Performance-based emergency landing trajectory planning applying meta-heuristic and Dubins paths

Hassan Haghighi, Daniel Delahaye, Davood Asadi

PII: S1568-4946(22)00024-2
DOI: https://doi.org/10.1016/j.asoc.2022.108453
Reference: ASOC 108453

To appear in: *Applied Soft Computing*

Received date : 23 October 2020
Revised date : 6 January 2022
Accepted date : 11 January 2022

Please cite this article as: H. Haghighi, D. Delahaye and D. Asadi, Performance-based emergency landing trajectory planning applying meta-heuristic and Dubins paths, *Applied Soft Computing* (2022), doi: https://doi.org/10.1016/j.asoc.2022.108453.

Performance-Based Emergency Landing Trajectory Planning Applying Meta-Heuristic and Dubins Paths

Hassan Haghighi[1] and Daniel Delahaye[2]
ENAC, University of Toulouse, 31400, France

and
Davood Asadi[3]
Adana Alparslan Türkeş Science and Technology University, Adana, 01250, Turkey

Emergency Landing is a complex problem of optimal path planning of an impaired airplane in presence of obstacles, while the airplane performance characteristics have degraded. Some in-flight failures can affect the airplane dynamics and therefore the new dynamic constraints must be considered in flight planning to the desired landing site. This paper introduces a novel hybrid form of Dubins-simulated annealing (HDSA) optimization framework for emergency landing. The proposed architecture applies Dubins paths and Apollonius' tangent line to generate candidate pieces of trajectories respecting the post-failure performance characteristics of the distressed airplane. The optimization pattern is used to select the optimal combination of the candidate trajectories based on the cost functions and the environmental constraints to lead the airplane to the desired landing site. Analytical performance-based equations are developed to achieve an admissible solution in emergency trajectory planning. The goal is to provide a general optimal framework, which can enhance the flight management system by assisting the pilot to plan the most suitable and admissible trajectory to the landing site in emergency flight conditions. The effectiveness of the proposed approach is demonstrated through simulations.

[1] Ph.D., Researcher, Optimization Department, ENAC.
[2] Professor, Head of Optimization Department, ENAC.
[3] Assistant Professor, Aerospace Engineering Department, Adana ATU.

Nomenclature

C_D = drag coefficient

C_L = lift coefficient

C_T = thrust coefficient

C_x = force coefficient in the *x*-direction

C_y = force coefficient in the *y*-direction

D = drag force (*N*)

$\delta_T, \delta_e, \delta_a, \delta_r,$ = thrust and control surface deflections (*deg*)

d*t* = time step (s)

F_W = weight force (*N*)

f, g, G, h = generic functions

ϕ, θ, ψ = Euler angles (roll, pitch, and yaw angles (*deg*))

γ = path angle (*deg*)

L = lift force (*N*)

m = aircraft total mass (*kg*)

n_T = total number of trajectories

n_{MT} = number of middle turns

O = reference map domain

O_{free} = allowable points on the map free of limitations

O_{guid} = map of guidance point

$O_{no.fly}$ = map of the forbidden area

O_{obs} = map of obstacle area

Ω = turn direction

$\mathbb{R}$ = real numbers and reference dimensional space

r_t = turning radius (*m*)

ρ = air density (kg/m^3)

s = line slope (*deg*)

S = reference aircraft area (m^2)

Tr = trajectory function

u , v = velocity in the *x* and *y* directions in body axes (*m/s*)

V_h = horizontal velocity in the inertial coordinate system (*m/s*)

V_a = aircraft total velocity (*m/s*)

V_g = aircraft glide velocity (*m/s*)

w = velocity in the *z*-direction in body axes (*m/s*)

W_x = wind velocity in the *x*-direction (*m/s*)

W_y = wind velocity in the *y*-direction (*m/s*)

W_z = wind velocity in the *z*-direction (*m/s*)

wp = waypoint position function

X_0 = initial position (*m*)

X_f = final position (*m*)

χ_0 = initial heading of aircraft (*deg*)

χ_f = runway orientation (*deg*)

i = time index during navigation

j = waypoint index

Subscripts

$0, i$ = initial condition

a = airplane parameter

f = final condition

max = maximum value of parameter

min = minimum value of parameter

x = *x* direction

y = *y* direction

z = *z* direction

I. Introduction

AN emergency condition is one in which the safety of the aircraft or persons is endangered for any reason. Emergency flight conditions may occur within or outside the aircraft that usually affect aircraft performance. In modern aviation, flight safety and risk reduction are important issues for manufacturers and passengers. In-flight failures in a transport aircraft can lead to significant performance degradation, loss of altitude or velocity, and undesired bank angles that may force the pilot to plan an emergency landing toward nearby suitable landing sites. One of the main challenges in emergency conditions is how to safely guide the airplane to the desired landing site. Due to the stressful and highly workload nature of the emergency conditions, it is not safe to expect the pilot to do this challenging task without the assistance of automation. Therefore, researchers are working on automation enhancement to help the pilot safely recovering the impaired airplane [1-5]. Automation can help by identifying and adapting to the failure and planning a new optimal landing trajectory that considers new constraints related to the airplane's degraded performance and landing requirements [4, 5].

In this paper, the problem definition is to generate an optimal path from an initial position and heading of X_0 and χ_0 , respectively, to a target runway with the desired position and direction of X_f and χ_f regarding the admissible post-failure turning direction and constraints. This problem arises when an emergency failure occurs during an urgent landing with no previous expected calculations. Path planning of an airplane is a non-trivial task, especially in the presence of obstacles and/or runway traffics, other landing requests, as well as uncertainty parameters such as wind field. Aerodynamic models can be used to plan flyable trajectories from an initial location to the desired airport runway. In this research, post-failure kinematic constraints including glide ratio and radius of turns as well as wind parameters are accounted for path planning toward the desired landing site. The kinematic constraints are derived for different bank angles and drag configurations due to power faults, actuator failure, or damage to lift generating surfaces.

The proposed architecture is presented after a brief review of the related literature. Degraded aircraft model, mathematical model, resolution algorithm for trajectory planning, and simulation results will be presented in the next sections. Finally, the conclusion section presents the key results of our research.

A. Previous Works and State of the Art

An emergency flight planner should be a necessary part of the Flight Management System (FMS) regarding numerous accidents caused by loss of thrust (i.e. AF447-2009, US airways 1549-2009), failure in control (Swissair 111-1998), structural damages (i.e. Northwest F85-B747-2002, Air Transat 961-A310-2005) and other failures, which leads to loss of control (LoC) [6-8]. It is essential to maintain stable flight in all flight conditions including the degraded performance conditions in presence of in-flight fault or failure. Some legal rules have been used to improve piloting ability by adjusting dynamic reference model characteristics (e.g., maximum bank/pitch rates) that are still within the performance envelope [9, 10]. The integration of a reference model into an intelligent flight controller has enabled pilots to maintain control of a damaged aircraft following an extensive suite of control surface and loss-of-thrust failure combinations [11, 12].

Finding the stable point of the flight envelope provided by the autopilot is an auxiliary element of the piloting system expected to maintain a stable flight during failure scenarios [4, 5]. Unmanned Aerial Vehicle (UAV) researchers have developed related flight management tools for fully autonomous operations [13]. A hierarchical analogous control architecture with different layers of strategic decision making, tactical planning, and reconfigurable flight control is presented in Refs. [14, 15]. Alternative offline route responds to anomalous events [16], dynamic programming [17, 18], flight plans from a database of trim conditions and maneuvers [4, 19], and control strategy are some innovative model-based approaches to enhance autonomy in post-failure flight conditions [20]. Despite the above approaches, there are still serious investigations regarding the required run-time, model accuracy, and real-time capability to govern the maneuvers toward the landing site during in-flight failure.

Generally, combinatorial methods based on path geometry have been primary tools for constrained path planning problems. The problem of finding the shortest path under the curvature constraint was first introduced in the pioneering work of Dubins [21]. Dubins paths are characterized as paths in two-dimensional obstacle-free space that could be classified into known permutations of bang-off-bang control sequences in three basic motions of left, straight, and right. This is a basic pattern for the researchers to study some extensions to the special application of geometrical methods in robotics such as tree-based investigations [22], classification, and obstacle shape [23, 24]. Dubins two-dimensional (2D) shortest paths have been previously applied to generate the shortest paths for an aircraft in a three-dimensional (3D) environment. Atkins [25] and some other researchers [26, 12] have applied Dubins paths to generate

3D trajectories for an emergency flight of an aircraft in different scenarios, while ignoring the presence of obstacles and uncertainties.

Several other methods such as grid base, Dijkstra, numerical Hamilton Jacobi, Eikonal equation, and meta-heuristic methods have been applied for path planning of moving vehicles with dynamic constraints in presence of obstacles [27-29]. The applicability of the aforementioned methods to aerial vehicles, especially in emergency conditions respecting high speeds of aerial vehicles and required safety, is still challenging. Depending on the complexity of the search space (dimensionality of the search space), a huge computational effort might be required to find a valid solution. Other applied path planning approaches include potential fields, visibility graphs, or roadmaps are studied in [30]. Application of these methods requires costly precomputing effort with inflexibility drawback for reacting to uncertainties, especially in emergency flight conditions. Despite the progress in aviation technology in recent years, there is still a lack of an efficient and fast method that respects post-failure dynamics and the performance of the airplane to help pilots in critical emergency flight conditions.

B. Proposed Architecture

This paper proposed the architecture for emergency landing trajectory planning is composed of three main sub-modules including:

1-Post-failure performance analysis;

2- Route generation pattern module, which generates a search space for middle turns based on the feasible post-failure path segments;

3- Optimization method to achieve a fast and safe landing trajectory toward the landing site in presence of obstacles.

According to Fig. 1, post-failure performance identifies the failure and dominant constraints, which are considered in trajectory planning and optimization. It also considers the distance and directions to candidate landing runways. The route generation module is based on the analytical version of the adopted Dubins feasible routes, which starts from the initial position and heading and ends up with the desired position and direction of the landing site based on admissible turning radius and rate of altitude change. This module connects a list of intended middle turns to avoid obstacles and adjust maneuvers respecting the wind field, obstacles, or some moving objects. A mathematical functional formulation of geometrical design is developed for the arbitrary number of desired middle turns. The

proposed optimization method is based on a Hybrid form of Dubins and Simulated Annealing (HDSA), while considering useful assumptions to create rapid optimal admissible trajectories.

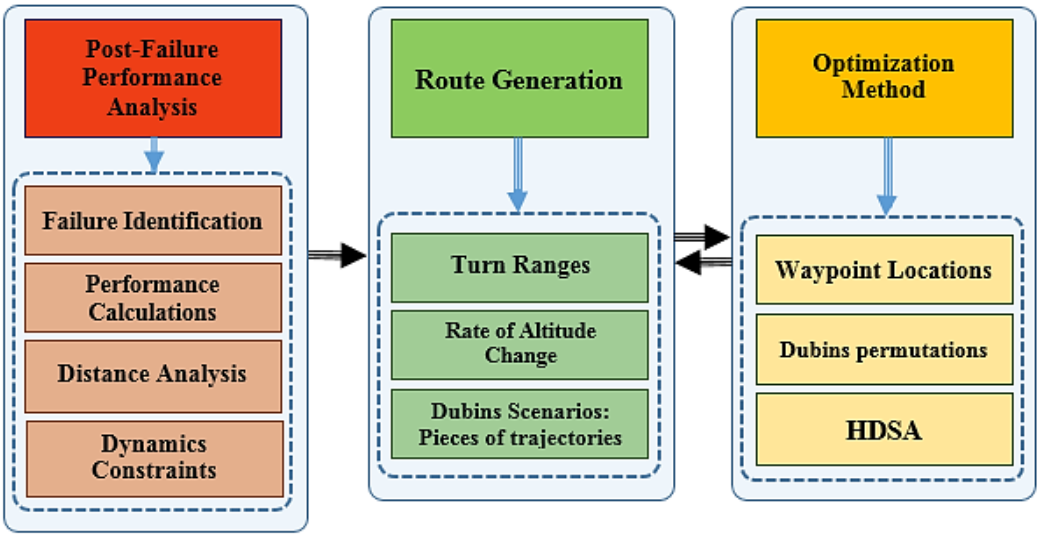

Fig. 1 Proposed architecture for emergency landing trajectory planning

II. Degraded Aircraft Model

The dynamic data of post-failure flight determines the airplane's dynamical constraints and maneuvering capabilities for trajectory planning. In emergency flight conditions like damage, actuator fault, or engine failure, where the airplane experiences a degraded performance or is confined to new kinematic constraints such as admissible one side turn (to left or right), undesired or higher radius of turn, while applying lower thrust force, and flying at lower speeds or altitudes, the approach flight plan to the desired runway must comply with the new performance constraints. In addition, the desired or undesired bank angle has a direct and fundamental effect on the glide ratio and the radius of rotation as one of the main parameters of the trajectory generation algorithm. During the cruise flight, the bank angle (ϕ) induces a downforce, $mg(1-\cos\phi)$ as a function of airplane local weight (mg) and it increases the gliding velocity and impact force during touch down. To derive the performance parameters, the airplane position and velocity are firstly defined as a three-dimensional vector in the inertial frame as Eq. (1).

$$\overrightarrow{r_a} = \begin{bmatrix} x \\ y \\ z \end{bmatrix}, \overrightarrow{V_a} = \begin{bmatrix} \dot{x} \\ \dot{y} \\ \dot{z} \end{bmatrix} = \begin{bmatrix} u \\ v \\ w \end{bmatrix} \tag{1}$$

Regarding the horizontal and vertical plane of the inertial axes, the velocity components can be expressed as functions of path angle (γ) and side angle (χ) as follows:

$$u = \left|\overrightarrow{V_a}\right| \cos\gamma \cos\chi \tag{2}$$

$$v = \left|\overrightarrow{V_a}\right| \cos\gamma \sin\chi \tag{3}$$

$$w = \left|\overrightarrow{V_a}\right| \sin\gamma \tag{4}$$

where $\left|\overrightarrow{V_a}\right| = \sqrt{u^2 + v^2 + w^2}$ is the airplane velocity and $\overrightarrow{r_a} = \int \overrightarrow{V_a}\, dt$ denote the location vector. In case of wind $\overrightarrow{W} = (W_x, W_y, W_z)$, the relative velocity becomes $\overrightarrow{V_a} + \overrightarrow{W} = (u + W_x, v + W_y, w + W_z)$ and the effective displacement is calculated according to $\overrightarrow{r_a} = \int \overrightarrow{V_a}\, dt$. Regarding the effect of failure or damage on the airplane, the distribution of lift (L), drag (D), path angle (γ), turning rate ($\dot{\chi}$) and radius (r_t) as well as thrust (T) and weight (F_W) become the key elements in landing performance analysis. Therefore, based on the post-failure constraints on the angles and the performance parameters, the following performance equations are derived:

$$L = F_w \cos\gamma \cos\phi = \frac{1}{2}\rho {V_a}^2 S\, C_L \tag{5}$$

$$D = F_w \sin\gamma \cos\phi = \frac{1}{2}\rho {V_a}^2 S\, C_D \tag{6}$$

$$\gamma = \operatorname{acot}\frac{u}{w} = \operatorname{acot}\frac{\Delta x}{\Delta h} = \operatorname{acot}\frac{L}{D} \tag{7}$$

$$\dot{\chi} = L\frac{\sin\phi}{m\, V_a \cos\gamma} = \frac{g \sin\phi}{V_a \cos\gamma} \tag{8}$$

$$r_t = \frac{\dot{\chi}}{V_a \cos\gamma} = \frac{2m}{\rho S}\sqrt{\frac{K}{C_{D0}}}\frac{\cos\gamma}{\tan\phi} \tag{9}$$

According to Eq. (7), the glide distance ($\sqrt{\Delta x^2 + \Delta h^2}$) is maximum when Δx is maximum, and accordingly when lift to drag ratio (L/D) is maximum. Regarding Eqs. (5) to (9), the angular rate of path angle and gliding velocity are derived as the following equations, where C_L , C_D and C_T are lift, drag, and thrust coefficient, respectively.

$$\dot{\gamma} = \frac{\frac{1}{2}\rho {V_g}^2 S(C_L + C_T \sin\alpha) - F_w \cos\gamma \cos\phi}{m V_g} = \frac{\dot{w}}{u(1 + \tan^2\gamma)} \tag{10}$$

$$V_g = \sqrt{\frac{2F_w}{\rho S \sqrt{{C_L}^2 + {C_D}^2}}} \tag{11}$$

Considering the airplane post-failure performance, the domain of four main parameters, velocity (V_a), turning radius (r_T or $\dot{\chi}$), path angle (γ), and bank angle (ϕ) must be considered in landing trajectory design. The trajectory planner constructs a valid post-failure waypoint sequence that can be safely followed to the landing runway. It must generate some segmented trajectories that are intuitive for pilots or air traffic control (ATC) but needs not to be optimized with the additional computational cost because the overriding goal is a safe landing. After indicating initial and final states, according to post-failure performance, the relevant Dubins paths of guaranteed minimum length are constructed to verify the reachability of the selected runway. According to the performance analysis of Eqs. (5) to (11), it is possible to calculate the airplane response when encountering a failure in terms of observed parameters.

A. Post-failure Scenarios

The aircraft follows a certain pattern in cruise and landings flights so that with a different configuration of the control surface, predictable responses are received from the aircraft. Therefore, the responses of the undamaged aircraft, which arise from a particular configuration of the control surface can be considered as a standard or trim condition during the landing. With the trim conditions and using Eqs. (5) to (11), the dynamic required forces to adapt to the post-failure conditions can be calculated.

Table 1-5 represent the post-failure performance factors of an A320 airplane in a landing situation at 225-knots approach speed in five main emergency cases. Lift reduction can be measured as a consequence of various defects by disturbing the local equilibrium and measuring the acceleration or velocity of the glide (rate of descending). Similarly, it is also possible to calculate an imbalance in the aircraft's overall drag and variation of overall speed or acceleration, to obtain the drag reduction failures. Other investigated failures such as induced bank angle, thrust reduction (or one-side engine thrust reduction) can be viewed or calculated directly through aircraft gauges and do not require other arguments. The first columns of tables denote the trim condition in the conventional landing of A320 airplane with zero percent of damages consequently, those are considered as the basic criteria for calculating other conditions.

These calculations of the following tables will be the input of trajectory planning as dynamic constraints and perform the basis for the development of the proposed algorithm in emergency flight conditions.

Table 1. Failure due to lift reduction, effect on the landing parameters (at 225-knot approach speed)

		Lift reduction								
		0%	5%	10%	15%	20%	25%	30%	35%	40%
$r_{t_{min}}$, m		± 2636	± 2775	± 2929	± 3101	± 3295	± 3515	± 3766	± 4056	± 4394
$\dot{\chi}_{max}$, *deg/s*	min	-2.45	-2.37	-2.25	-2.12	-1.99	-1.87	-1.75	-1.62	-1.5
	max	+2.45	+2.37	+2.25	+2.12	+1.99	+1.87	+1.75	+1.62	+1.5
$\dot{v}_g, m/s^2$		0	0.49	0.98	1.47	1.96	2.45	2.94	3.43	3.92
γ, *deg*		3.32	-	-	-	-	-	-	-	-
$\dot{\gamma}$, *deg/s*		0	-0.24	-0.49	-0.73	-0.97	-1.21	-1.46	-1.7	-1.95
Glide ratio		17.25:1	17.16:1	17.06:1	16.97:1	16.88:1	16.79:1	16.69:1	16.61:1	16.52:1
ϕ_{max} , *deg*		±30	±30	±30	±30	±30	±30	±30	±30	±30

Table 2. Failure due to induced bank angle caused by control surface failure, effect on the landing parameters (at 225-knot approach speed)

		Induced bank angle (left side)								
		0,deg	5,deg	10,deg	15,deg	20,deg	25,deg	30,deg	35,deg	40,deg
$r_{t_{min}}$, m	Left	± 2636	-2636	-2636	-2636	-2636	-2636	-2636	-2432	-2090
	Right		+3179	+3928	+5191	+7737	+15416	+∞	-3179	-3928
$\dot{\chi}_{max}$, *deg/s*	min	-2.45	-2.45	-2.45	-2.45	-2.45	-2.45	-2.45	-2.81	-3.15
	max	+2.45	+2.07	1.67	+1.27	+0.85	+0.43	0	-2.07	-1.67
$\dot{v}_g, m/s^2$		0	0.04	0.15	0.33	0.59	0.92	1.31	1.77	2.30
γ, *deg*		3.32	-	-	-	-	-	-	-	-
$\dot{\gamma}$, *deg/s*		0	-0.02	-0.07	-0.17	-0.29	-0.46	-0.65	-0.88	-1.14
Glide ratio		17.25:1	17.24:1	17.23:1	17.21:1	17.19:1	17.16:1	17.12:1	17.08:1	17.03:1
ϕ_{max} , deg		±30	- 30,+25	- 30,+20	- 30,+15	-30,+10	-30,+5	-30,0	-35,-5	-40,-10

Table 3. Effect of thrust reduction in landing parameters (at 225-knot approach speed)

		Landing Thrust reduction								
		0%	5%	10%	15%	20%	25%	30%	35%	40%
$r_{t_{min}}$, m		± 2636	± 2425	± 2177	± 1941	± 1720	± 1511	± 1317	± 1135	± 967
$\dot{\chi}_{max}$, *deg/s*	min	-2.45	-2.71	-3.02	-3.39	-3.82	-4.35	-4.99	-5.79	-6.80
	max	+2.45	+2.71	+3.02	+3.39	+3.82	+4.35	+4.99	+5.79	+6.80
$\dot{v}_g, m/s^2$		0	0.49	0.98	1.47	1.96	2.45	2.94	3.43	3.92
γ, *deg*		3.32	-	-	-	-	-	-	-	-
$\dot{\gamma}$, *deg/s*		0	-0.24	-0.49	-0.73	-0.97	-1.21	-1.46	-1.7	-1.95
Glide ratio		17.25:1	17.16:1	17.06:1	16.97:1	16.88:1	16.79:1	16.69:1	16.61:1	16.52:1

Table 4. Effect of drag reduction on landing parameter caused by a failure in landing gear or control surface (at 225-knot approach speed)

		Drag reduction								
		0%	5%	10%	15%	20%	25%	30%	35%	40%
$r_{t_{min}}$, m		± 2636	± 2977	± 3318	± 3719	± 4199	± 4777	± 5484	± 6360	± 7464
$\dot{\chi}_{max}$, *deg/s*	min	-2.45	-2.27	-2.09	-1.92	-1.75	-1.59	-1.43	-1.28	-1.14
	max	+2.45	+2.27	+2.09	+1.92	+1.75	+1.59	+1.43	+1.28	+1.14
$\dot{v}_g, m/s^2$		0	-0.52	-1.09	-1.73	-2.45	-3.27	-4.2	-5.28	-6.54
γ, *deg*		-3.32	-	-	-	-	-	-	-	-
$\dot{\gamma}$, *deg/s*		0	0.26	0.54	0.86	1.22	1.62	2.09	2.62	3.25
Glide ratio		17.25:1	17.3:1	17.36:1	17.42:1	17.49:1	17.57:1	17:66:1	17.77:1	17.90:1
ϕ_{max} , *deg*		±30	±30	±30	±30	±30	±30	±30	±30	±30

Table 5. Effect of asymmetric thrust (one side engine thrust reduction) on landing parameters (at 225-knot approach speed)

		One side power reduction (left engine)								
		0%	10%	15%	20%	25%	30%	35%	40%	100%
$r_{t_{min}}$,*m*		± 2636	± 2553	± 2486	± 2418	± 2351	± 2284	± 2217	± 2150	± 1344
$\dot{\chi}_{max}$, *deg/s*	min	-2.45	-2.51	-2.55	-2.58	-2.62	-2.66	-2.7	-2.74	-3.46
	max	+2.45	+2.51	+2.55	+2.58	+2.62	+2.66	+2.7	+2.74	+3.46
$\dot{v}_g, m/s^2$		0	0.49	0.74	0.98	1.23	1.47	1.72	1.96	4.91
γ, *deg*		-3.32	-	-	-	-	-	-	-	-
$\dot{\gamma}$, *deg/s*		0	-0.24	-0.37	-0.49	-0.61	-0.73	-0.85	-0.97	-2.44
Glide ratio		17.25:1	17.20:1	17.18:1	17.16:1	17.13:1	17.11:1	17.09:1	17.06:1	16.79:1
ϕ_{max} , *deg*		±30	±30	±30	±30	±30	±30	±30	±30	±30

III. Mathematical Model

Post-failure investigations and related trajectory design are challenging problems that require specific mathematical formulation. The input data can be categorized into two sections of environmental and aircraft data. In fact, decision variables are a combination of mentioned categories that have a strong impact on trajectory design for specific purposes such as emergency landing. Regarding the mathematical model and optimization algorithm, problem structure can be defined based on the decision variables, constraints, and objectives in the proposed post-failure trajectory generation.

A. Decision variables

Decision variables are divided into two categories: dynamics variables and geometric variables. Dynamic variables are related to the aircraft performance data during the post-failure operations, while geometric variables are the external factors that affect the structure of the generated path. These variables are related to how the problem is viewed and how it is solved. The dynamic variables are mainly based on minimum turning radius ($r_{t_{min}}$) and rate of descend ($\dot{v}_g$), which directly related to the airplane velocities, flaps, thrust, and control surface configuration ($\delta_f, \delta_T, \delta_e, \delta_a, \delta_r$), Euler angles ($\phi, \theta, \psi$), and post-failure performances. The geometric variables as the external terms are initial and final positions and headings ($(\bar{X}_0, \bar{\Theta}_0) = (x_0, y_0, z_0, \chi_0, \gamma_0)$, $(\bar{X}_f, \bar{\Theta}_f) = (x_f, y_f, z_f, \chi_f, \gamma_f)$), number of middle turns (n_{MT}), position of obstacles (O_{obs}: $(x, y, z) \in O$ as reference environment) and wind field ($\vec{W}(w_x, w_y, w_z)$) parameters.

B. Constraints

There are two types of constraints: dynamic and environmental constraints. Dynamic constraints are related to the aircraft post-failure performance that includes velocities ($V_a(u, v, w = -v_g)$), angular rates ($\dot{\chi}, \dot{\gamma}$), glide ratio ($\tan\gamma$),

minimum turning radius ($r_{t_{min}}$) and turning direction (Ω) when the only special turn is permitted (Eqs. (12) to (15)). The environmental constraints are related to the effective external factors such as minimum flight altitude ($h = -z > h_{runway}$), runway orientation or distance, forbidden area, obstacles, and some uncertainty like allowable crosswind or wind velocity. The results must be calculated according to the mentioned constraints.

$$V_{a_{min}} \leq V_a \leq V_{a_{max}}, \dot{v_g} \geq 0 \tag{12}$$

$$|\dot{\chi}| \leq \dot{\chi}_{max}, \dot{\gamma} \geq 0, 0 \leq \gamma \leq \gamma_{max} \tag{13}$$

$$|r_{t_{min}}| \geq r_{t_0} \tag{14}$$

$$h \geq h_{runway}, (\bar{X}_f, \bar{\Theta}_f) = \left(x_f, y_f, z_f, \chi_f\right) \tag{15}$$

C. Objectives

The main objective is to generate safe landing trajectories based on aircraft post-failure performance characteristics, which are practically implementable respecting the solution accuracy and run-time. The important parameters considered in trajectory planning include minimum traveling distance, minimum turn, obstacle avoidance, and flight in minimum crosswind conditions regarding windy situations. To decrease the run-time and increase solution accuracy, the structure of the problem should be defined as a single objective problem as a function of initial, final, and middle waypoints (wp), radius of turns (r_t), descending rate ($\dot{\gamma}$), velocity, and turning directions as follows.

$$G = \int_{X_0}^{X_f} dX = \int_{X_0}^{X_f} (\overrightarrow{V_a} + \overrightarrow{W}) dt \tag{16}$$

$$G = Tr(wp, r_t, \dot{\gamma}, \overrightarrow{V_a} + \overrightarrow{W}, \Omega) \tag{17}$$

In summary, the problem-solving structure is a combination of decision variables, constraints, and objectives that must be gathered in the solution method.

D. Trajectory generation

It is necessary to generate a general framework to make a relation between the main variables and objectives to find a suitable resolution algorithm and a clear expression of the cost function. Let $O \subseteq \mathbb{R}^3$ represents a bounded and connected domain of a 3D terrain map. The interior boundary of the orientation map like the Operational Navigation Chart (ONC) is partitioned into obstacle space (O_{obs}), no-fly zone ($O_{no.fly}$), free space (O_{free}), and guidance points

(O_{guid}) or the spots that must be covered such as NDB antenna such that; $O_{obs} \cap O_{no.fly} \cap O_{free} \cap O_{guid} = O$. The location of any point on the map will be noted as $\bar{X}$: $(x, y, z) \in O$. According to the curved-based nature of the designed guidance route, each trajectory point is specified by the horizontal (χ) and vertical (γ) turning angles ($\bar{\Theta} = (\chi, \gamma)$) respecting the inertial plane. Therefore, each point is represented as $(\bar{X}, \bar{\Theta}) = (x, y, z, \chi, \gamma) \in O \times [0,2\pi)^2$. Depending on the airplane feasible descending rate, which is dictated by the airplane's post-failure performance constraints $[\gamma_{min}, \gamma_{max}]$, the trajectory can be expressed as a one-dimensional rotation: $(\bar{X}, \bar{\Theta}) = [X_{min}, X_{max}]^3 \rightarrow O \times [\chi_{min}, \chi_{max}]$ by having a constant descending rate. In fact, the constant vertical turning angle of the airplane is constrained between the steepest descent angle (γ_{min}) and the best-glide angle γ_{max}. The horizontal turning angle of the trajectory χ, which determines the trajectory radius of turn (r_t), is governed by the velocity components as below:

$$\chi = \operatorname{atan}\left(\frac{\dot{y}}{\dot{x}}\right) \tag{18}$$

Regarding Eq. (18), the feasible trajectory depends on new performance characteristics of the airplane in the admissible space of $O_{free} \times [\chi_{min}, \chi_{max}]$. If χ is differentiable in the domain O, the turning radius is represented as:

$$r_t = \frac{\sqrt{\dot{x}^2 + \dot{y}^2}}{\dot{\chi}} = \frac{\sqrt{u^2 + v^2}}{\dot{\chi}} = \frac{V_h}{\dot{\chi}} \tag{19}$$

The minimum turning angle is a parameter, which depends on airplane post-failure performance characteristics of bank angle (ϕ) as below:

$$L \cos\phi = F_W \tag{20}$$

$$r_t = \frac{m{V_h}^2}{L \sin\phi} = \frac{m{V_h}^2}{F_W \tan\phi} \tag{21}$$

where V_h is the velocity in the horizontal direction of the inertial plane, L and F_W represent the total airplane's lift and weight force, respectively. Accordingly, the minimum radius of turn $r_{t_{min}} = {V_h}^2/g \tan\phi_{max}$ is a function of performance factors, where $\tan\phi = L/D$. Therefore, $r_{t_{min}}$ is a function of $(L/D)_{max}$ as the main performance parameter. When an aircraft is in an emergency flight condition, all the above parameters should be estimated. Depending on the distribution of the lift and drag force, other performance parameters can be locally calculated.

Since the rotation of the airplane takes place on circular arcs, it is necessary to make some observations and calculations in this case through the results of Apollonius' problem [31].

Definition 1: Two directions of rotation around the circumference can be assigned to each assumed circle on the plane, counter-clockwise (CCW) for a positive direction of rotation and clockwise (CW) that indicates the negative direction.

Theorem 1: Two directional circles and a directional line are tangents whenever their lines and non-directional circles are tangent to each other and all of the directions are the same at the tangent point.

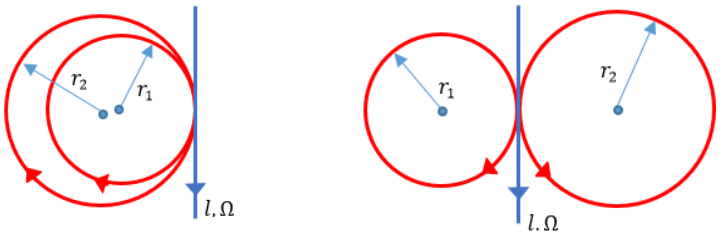

(a) (b)

Fig. 2 Tangent theorem related to aircraft turning radius (r) and orientation (Ω), (a): external tangent line, (b): internal tangent line.

According to theorem 1, it can be concluded that there is only one tangent between the two directional circles as shown in Fig. 2. If the rotation direction of the circles is the same, the tangent is an external tangent, otherwise, it is an internal tangent. In addition, there are only two tangents between a directional circle and a directionless circle: one internal tangent and one external tangent that indicate different lengths of the traveling path. Moreover, for two circles without a default direction of rotation, there are four tangents, each tangent creating a certain rotation on the desired circles as illustrated in Fig. 3. Let $\hat{e} = \alpha\hat{\imath} + \beta\hat{\jmath}$ be a unit vector of directional tangent line in a tangent point of a circle. If the relative angle of tangent point to the center of rotation in inertial axis is θ, the direction of rotation Ω is as follow:

$$\Omega = \hat{e}_\theta = -\alpha \sin\theta + \beta \cos\theta \tag{22}$$

where $\Omega = +1$ denotes the CCW direction of rotation and $\Omega = -1$ denotes CW rotation.

Theorem 2: A hypothetical heading direction on the plane of rotation with a certain radius creates two tangent circles on the same plane with different rotational directions (Fig. 3*a*).

According to theorems 1 and 2, for the emergency problem with given initial and final desired positions and headings, there are four possible trajectories to transfer from any directional location A to B as shown in Fig. 3*b* (noted 1, 2, 3, and 4).

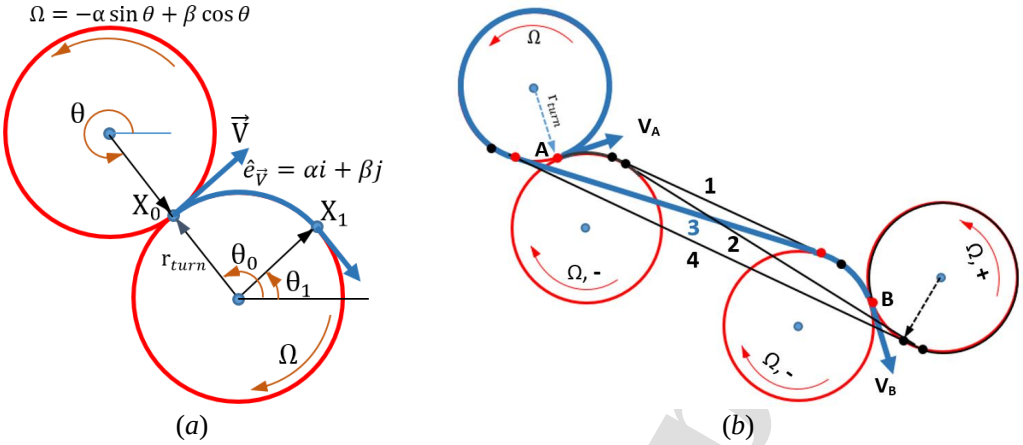

Fig. 3 Turning parameters, (*a*): possible turn assigned to the heading and parameters, (*b*): four possible traveling routes (lines 1 to 4) between two given headings, blue line one candidate tracking route.

E. Dubins Middle Turns

From the mathematical point of view, with at least two rotations and one straight line, it is possible to make a path between two arbitrary vectors. Sometimes, in order to satisfy a specific purpose, it is necessary to use more than two rotations, in which the middle turns are used. In fact, when it is not possible to cross a straight path, only adding middle turns, adding another rotation circle, keeps us in the optimal state that should be considered as an extension of the simple Dubins mode. Middle turns are required to be defined in landing trajectory planning for several reasons. In general, middle turns can be used for planning a smooth path to avoid obstacles, moving efficiently in the wind field, or unstable moving weather, as well as crossing a longer distance to reduce the flying altitude.

The middle turns are composed of turning circles as illustrated in Fig. 4, which are used in the turn maneuver to minimize the cost. As it is illustrated, adding one or more middle circles can reduce the traveling distance, where it can pass around the obstacles with a shorter distance. In this approach, n_{MT} denotes the number of middle turns, therefore, the total number of traveling routes (n_T) as the total tangent between circles, can be calculated as:

$$\begin{aligned} n_{MT} = 0&: n_T(0) = 4 \times 1 = 4 \\ n_{MT} = 1&: n_T(1) = 4 \times 2 = 8 \\ n_{MT} = 2&: n_T(2) = 4 \times 4 = 16 \end{aligned} \tag{23}$$

$$n_{MT} = n: n_T(n) = 4 \times 2^n = 2^{n+2}$$

$$n_T(n) = 2\, n_T(n-1) \tag{24}$$

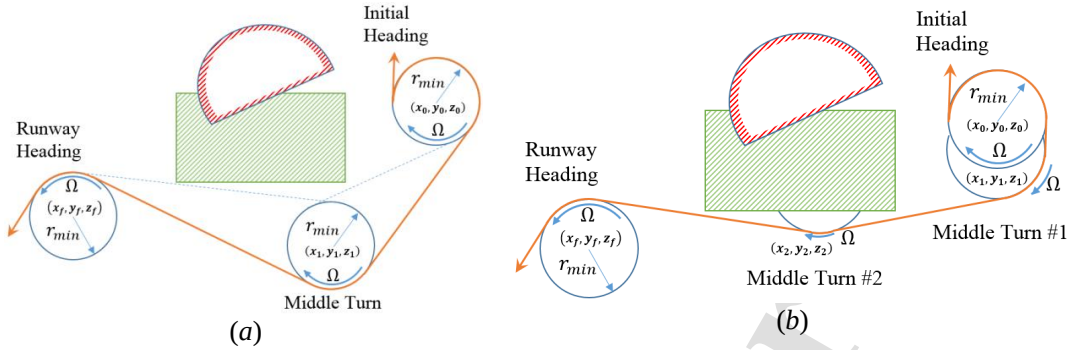

Fig. 4 Middle turn approach, (*a*) one middle turn, (*b*) two middle turns.

Lemma1: There are four tangent paths for rotations caused by non-directional and non-intersecting circles (as shown in Fig. 5), and only two external tangent paths will exist if the circles are intersecting. The tangent points are used as the waypoints for deriving smooth trajectories.

For tangents between two circles in parametric solution in the plane of rotation, suppose x_0, y_0, and r_0 is the center point and radius of the first circle, and x_1, y_1, and r_1 is the center and radius for the second one. According to Fig. 5, suppose that point $(x, y) = (a, b)$ is the tangent location on the first circle, then point $(x, y) = (c, d)$ is the tangent location on the second circle in the two-dimensional plane, and s is the tangent line slope.

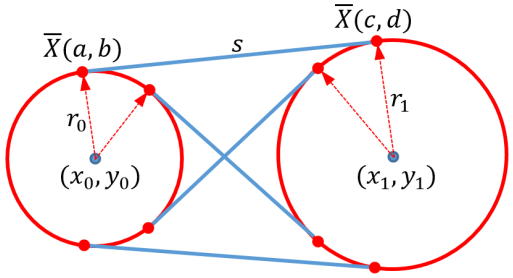

Fig. 5 Tangent theorem between two non-rotational circles according to the lemma 1.

According to equations of line and circles, a set of 5 nonlinear algebraic equations can be determined for *a*,*b*,*c*,*d*,*s* as variables in terms of given parameters x_0, y_0, r_0, x_1, y_1, r_1 for every two arbitrary circles in parametric form as follows:

$$\begin{cases} \boldsymbol{d}-\boldsymbol{b}=\boldsymbol{s}(\boldsymbol{c}-\boldsymbol{a}) \\ \boldsymbol{b}-y_0=-\dfrac{1}{\boldsymbol{s}}(\boldsymbol{a}-x_0) \\ \boldsymbol{d}-y_1=-\dfrac{1}{\boldsymbol{s}}(\boldsymbol{c}-x_1) \\ (\boldsymbol{a}-x_0)^2+(\boldsymbol{b}-y_0)^2={r_0}^2 \\ (\boldsymbol{c}-x_1)^2+(\boldsymbol{d}-y_1)^2={r_1}^2 \end{cases} \tag{25}$$

The above parametric equations must be solved to reach the equations of tangent straight lines and more importantly the location of tangent points in the inertial orientation. Eq. 25 has the analytical solution that derives the possible tangents between two turns during trajectory planning. Since there are four tangent lines in separated circles (two outers and two crossovers) and two tangent lines in intersecting circles (only two outer tangents), the nonlinear set of equations presented in Eq. 25 has four real solutions for separated circles and two real solutions for intersecting circles. The solution can be extended to the desired number of middle turns in terms of directional or directionless circles.

F. Simulated Annealing

Simulated Annealing (SA) is an iterative meta-heuristic algorithm for solving non-convex and nonlinear optimization problems [32]. As a metallurgical annealing imitation, a search with SA begins with an initial temperature $T_{initial}$ sufficiently large to permit a search of a wide area and ends with a terminal temperature $T_{terminal}$ sufficiently small to follow the steepest descent heuristic in moving global minimums [33]. The solution at an iteration i is X_i, while $f(X_i)$ denotes the corresponding objective function, which represents the related cost value of X_i in generic form. The likelihood that the subsequent solution X_{i+1} is found at a random solution proximate to X_i, with updated solutions $X_i{}'$ created by randomly searching in the domain. The relative cost change between X_i and $X_i{}'$ is expressed as Eq. (26).

$$\Delta f_i=\frac{f(X_i{}')-f(X_i)}{f(X_i)} \tag{26}$$

Beginning with the initial solution, which results in smaller cost value than the previous solution $f(X_i')<f(X_i)$ is always accepted. When $f(X_i')\geq f(X_i)$, $X_i{}'$ will be accepted as the new current solution with the probability $\Pr_i(\Delta f_i,T_k)=\exp(-\Delta f_i/T_k)$. We can define the admissible probability, p_0, a probability number in the range of [0,1], to accept or decline new solutions, where the greater numbers denote a stronger probability of solution.

$$\Pr_i(\Delta f_i, T_k) = \begin{cases} \exp\left(-\frac{\Delta f_i}{T_k}\right) & \Delta f_i \geq 0 \\ 1 & \Delta f_i < 0 \end{cases} \tag{27}$$

$$X_{i+1} = \begin{cases} X_i' & \Pr_i \geq p_0 \\ X_i & otherwise \end{cases} \tag{28}$$

where T_k is the temperature at the k_{th} step of going through with the degraded solution $\Delta f_i \geq 0$ that enables the solution to avoid the local minimum relates. It also allows for analysis of the whole part of the solution space affecting the cost value control parameter. The value of T decreases exponentially with the probability function as given in Eq. (29).

$$\lim_{T \to 0} \exp\left(-\frac{\Delta f_i}{T_k}\right) = 0, \ \Delta f_i > 0 \tag{29}$$

Therefore, as the value of T decreases, the probability of accepting a degraded solution also decreases. The following cooling schedule is adopted as Eq. (30).

$$T_{k+1} = \alpha \, T_k \tag{30}$$

where α denotes the cooling rate, which is a value between 0 and 1.

The algorithm explores one neighborhood at each iteration, which is selected among previously defined neighbors. The neighbor $N(X_i)$ consists of various types of selecting functions implemented by randomly selecting a solution node from index i in solution space X with a probability proportional to the size of the neighbors [34]. The neighbors enable the solution to move toward a feasible solution based on the control parameter T. By analogy, the principle of neighbor generation corresponds to the perturbation mechanism, and the principle of acceptance represents two stages: generation and acceptance.

IV. Resolution Algorithm

The main resolution is based on the two simultaneous methods of trajectory generation and optimization. As a novel approach, trajectory generation applies the desired number of middle turns to produce the optimized tangent lines and turns for different purposes such as avoiding the obstacles, reducing the flight altitude to approach a runway altitude, or flying in the wind fields. Dubins routes, an expanded solution for connecting several middle turns and Apollonius problem, are derived from the post-failure constraints of the airplane. These two steps are merged into our proposed hybrid form of Dubins trajectory generation by applying the simulated annealing algorithm in the outer optimization loop to find the best turns locations and parameters. Since the turns themselves are dynamical elements,

they combine well with the aircraft post-failure dynamic problem and produce an integrated geometric framework of path planning.

A. Hybridization of Dubins and Simulated Annealing

Trajectory planning is the optimal solution of admissible waypoints in the domain of airplane performance and maneuverability. Based on the HDSA approach, a kind of optimal trajectories can be produced in an emergency landing procedure. According to section II, emergency landing is executed in two levels; 1- generation of candidate trajectories applying the Dubins paths, which respect the airplane post-failure performance characteristics and 2- selecting and matching the optimal trajectories among the generated ones respecting the landing cost functions and environmental limitations by implementing the simulated annealing algorithm. Let Tr_m^n be the candidates' trajectories calculated from Dubins waypoints (wp_i), minimum admissible turning radius ($r_{t_{min}}$), path angle angular velocity ($\dot{\gamma}$), and airplane landing velocity (V_a) as Eq. (31):

$$Tr_m^n = \bigcup_{j=1}^{n}\left[\sum_{i=1}^{m} f^j\left({wp_i}^j, {r_{t_{min}}}_i^j, \dot{\gamma}_i^j, {V_a}_i^j, \Omega_i^j\right)\right] \tag{31}$$

where n is the number of nominated Dubins trajectories, m is the number of Dubins composed sections, $wp_i = [x_i \quad y_i \quad z_i]' \subseteq O_{free}$ while $r_{t_{min_i}}, \dot{\gamma}_i$ and V_{a_i} belong to the airplane post-failure controllable flight envelope, and Ω_i denotes the rotation directions. The number of waypoints (m) for every nominated trajectory, the total numbers of waypoints for the entire solution domain (N_m) in terms of the number of middle turns (n_{MT}) and the total number of traveling routes ($n = 2^{n_{MT}+2}$) are as follows:

$$m = 4 + 2n_{MT} \tag{32}$$

$$N_m = n\,m = 2^{n_{MT}+2}(4 + 2n_{MT}) \tag{33}$$

$$N_m = 2^{n_{MT}+4} + n_{MT}\,2^{n_{MT}+3} \tag{34}$$

Accordingly, the Dubins principle covers the governing function of trajectories to two separate geometrical functions f_1 and f_2 as follows:

$$f\left(wp_i = \begin{bmatrix} x_i \\ y_i \\ z_i \end{bmatrix}, r_{t_{min_i}}, \dot{\gamma}_i, V_a, \Omega_i\right) = f_1\left(wp_i, wp_{i+1}, wp_{i+2}, r_{t_{min_i}}, \Omega_i\right) + f_2(\dot{\gamma}_i, V_a, \Omega_i) \tag{35}$$

$$f_1 = f_1\left(\begin{bmatrix} x_i \\ y_i \\ z_i \end{bmatrix}, \begin{bmatrix} x_{i+1} \\ y_{i+1} \\ z_{i+1} \end{bmatrix}, \begin{bmatrix} x_{i+2} \\ y_{i+2} \\ z_{i+2} \end{bmatrix}, r_{t_{min_i}}, \Omega_i\right) \tag{36}$$

$$f_1 = Cir\left(\begin{bmatrix} x_i \\ y_i \\ z_i \end{bmatrix}, \begin{bmatrix} x_{i+1} \\ y_{i+1} \\ z_{i+1} \end{bmatrix}, r_{t_{min_i}}, \Omega_i\right) + Lin\left(\begin{bmatrix} x_{i+1} \\ y_{i+1} \\ z_{i+1} \end{bmatrix}, \begin{bmatrix} x_{i+2} \\ y_{i+2} \\ z_{i+2} \end{bmatrix}\right) \tag{37}$$

$$f_2 = f_2\left(\sin\left(\int_{t_i}^{t_{i+1}} \dot{\gamma}_i \, dt + \gamma_{i_0}\right) V_a \, (t_{i+1} - t_i)\right) \tag{38}$$

$$(t_{i+1} - t_i) = \int_{\chi_i}^{\chi_{i+1}} \frac{r_{t_{min_i}} \, \mathrm{d}\chi}{V_a} \tag{39}$$

According to Eq. (35), it is assumed that a 3D trajectory is a separate combination of two functions f_1 and f_2, one for generating the path through Dubins solution and the other for the effect of the 3D equations. Equations (36) to (39) represent the terms of the trajectory where Cir and Lin denote the curvature and linear sections of the trajectory, respectively. Let $\bar{X}$ be a point on the circumference of a rotation arc and χ_X be a corresponding angle to the origin of the inertial axis, the curve part of the rotation as the arc of the circle follows the following geometric structure.

$$Cir(\bar{X}_i, \bar{X}_{i+1}, r\,, \Omega) = \begin{cases} \bar{X}: \ |\bar{X}_{i+1} - \bar{X}_i| - r_{t_{min_i}} = 0 \\ \chi: \ \left(1 - sgn\left(\chi_{\bar{X}_{i+1}} - \chi_{\bar{X}_i}\right)\Omega_i + \right)\pi + \Omega_i\left(\chi_{\bar{X}_{i+1}} - \chi_{\bar{X}_i}\right) \end{cases} \tag{40}$$

For the linear part of trajectories (Lin) regarding the position vector ($\vec{r}_a$), there is an independent scalar parameter (t) that represents a movement from an initial position ($\vec{r}_0 = [x_i \ \ y_i \ \ z_i]'$) with a specified step vector $\vec{a}$ to a local position $\vec{r}_a = \vec{r}_0 + \vec{a}$ where $\vec{a} = t\left(\vec{r}_{\bar{X}_{i+1}} - \vec{r}_{\bar{X}_i}\right)$. This term can be expanded as follows:

$$Lin(\bar{X}_i, \bar{X}_{i+1}) = \ \vec{r}_a = \vec{r}_{\bar{X}_i} + t\left(\vec{r}_{\bar{X}_{i+1}} - \vec{r}_{\bar{X}_i}\right) \tag{41}$$

$$Lin(\bar{X}_i, \bar{X}_{i+1}) = \langle x_i\,, y_i\,, z_i \rangle + t\langle x_{i+1} - x_i\,, y_{i+1} - y_i\,, z_{i+1} - z_i \ \rangle \tag{42}$$

Therefore, huge numbers of waypoints and candidate trajectories are generated to be selected as the inputs of the optimization algorithm, *i.e* simulated annealing. In fact, the process of aircraft optimal path planning in an emergency flight condition involves two parts: route generation and optimization. Although the Dubins process uses an internal optimization structure, it has been applied just as a route generation module, which can be integrated with a route optimization algorithm. The proposed design process uses SA to create an optimal trajectory Tr^* as follows:

$$Tr^* = Dubins\big(SA(r_t, \gamma, V_a, \bar{X}, m)\big) = Dubins(r_t{}^*, \gamma^*, V_a{}^*, \bar{X}^*, m^*) \tag{43}$$

where SA uses a path planner cost function $\mathcal{F}(Tr) \longrightarrow \mathcal{F}(Tr^*)$ to approach some specific trends. Therefore, the optimal trajectory applies a feedback process, which considers the dynamics, environment ($\bar{X}$, obstacles, winds, …), post-failure analysis (r_t, γ, V_a) , and peripheral parameters (m and algorithm parameters). The proposed HDSA architecture along with the algorithm description is summarized and presented in Figs. 6 and 7, respectively.

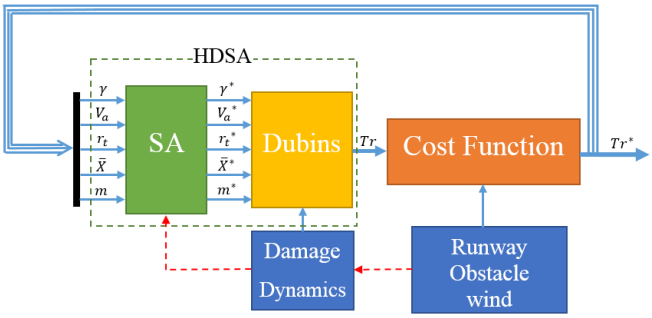

Fig. 6 Proposed HDSA and relation with post-failure constraint and environmental parameters.

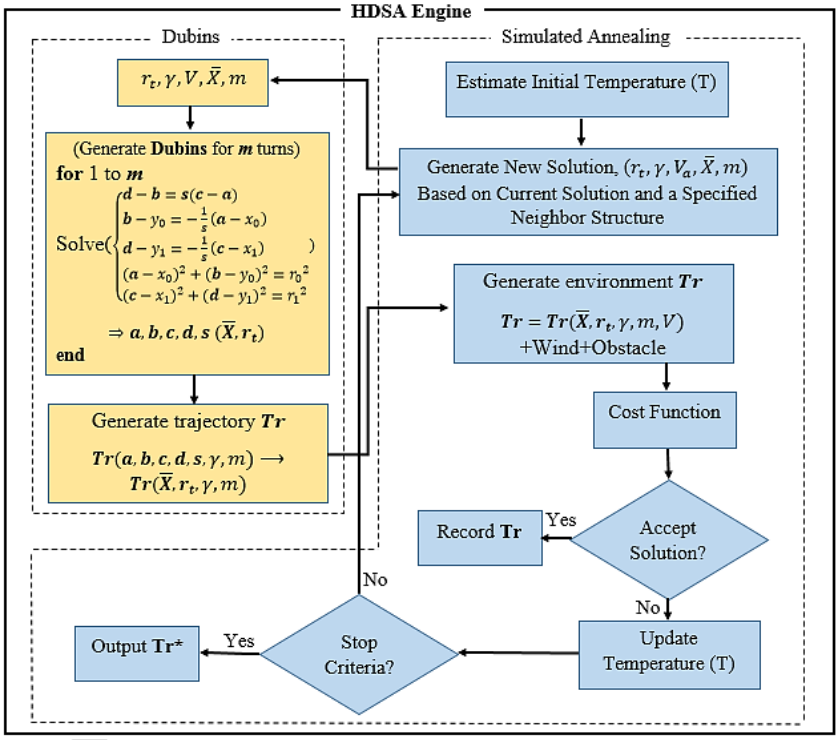

Fig. 7 Proposed HDSA engine, the hybridization of trajectory generation and meta-heuristic optimization.

B. Solution Coding

Let rewrite the trajectory according to dynamics parameters:

$$Tr^* = F(r_t{}^*, \gamma^*, V_a{}^*, \bar{X}^*, m^*) = min\left[G\left(\bigcup_{j=1}^{n}\left[\sum_{i=1}^{m} f^j\left(wp_i{}^j, r_{t_{min_i}}{}^j, \dot{\gamma}_i^j, V_{a_i}{}^j, \Omega_i^j\right)\right]\right)\right] \tag{44}$$

$$G(s,t) = h\big(s(t_f), t_f\big) + \int_0^{t_f} g(s,t)dt \tag{45}$$

Given that the Dubins structure ensures access to the end waypoint and direction, it can be written:

$$h\big(s(t_f), t_f\big) = h_1\left(s(t_f)\right) + h_2(t_f) \tag{46}$$

$$h_1\left(s(t_f)\right) = 0 \tag{47}$$

$$h\big(s(t_f), t_f\big) = h_2(t_f) = h(t_f) \tag{48}$$

if t_f is free, the $G(s,t)$ can be written only in integration form, while it guarantees the final states ($s(t_f)$) according to Dubins trajectory design. The concept of optimization is about the emergency landing, therefore, the post-failure dynamic determines $\dot{\gamma}$, V_a and Ω and enforce some restrictions on $r_{t_{min}}$. Accordingly, the cost function $G(s,t)$ can be rewritten to determine the optimal value of middle waypoints ($i = 2,3,\dots,(m-1)$) as the function of post-failure states $s = \left[wp_i{}^j, r_{t_{min_i}}{}^j\right]^T$ as Eqs (49) and (50).

$$G(s,t) = h(t_f) + \int_0^{t_f} g(s)dt \tag{49}$$

$$G(s,t) = \int_0^{t_f} g(\begin{bmatrix} x^j \\ y^j \\ z^j \end{bmatrix}, r_{t_{min}}{}^j)dt \;; \begin{cases} t_f = free \\ j = 1,2,\dots,n \end{cases} \tag{50}$$

If the criterion for selecting the solution states is the allowable sample space parameter of the aircraft post-failure dynamics, the cost function can be introduced based on a specific function and several constraints. Additionally, obstacle avoidance restrictions can be defined as a set of penalty functions. This point of view tends to simplify the problem-solving system and generally uses real structures. The efficient and optimal landing in an emergency condition depends on minimum traveling distance related to the obstacles and wind direction $\vec{W} = (W_x, W_y, W_z)$. Therefore, the following equations are considered as a cost function and related constraints.

$$g(X, r_{t_{min}}) = dis\left(f\left(wp_i, r_{t_{min_i}}, \dot{\gamma}_i, V_a, \Omega_i\right)\right) - dis(\overrightarrow{W}) \tag{51}$$

$$g(X, r_{t_{min}}) = dis\left(f\left(wp_i, r_{t_{min_i}}, \Omega_i\right)\right) - dis(\overrightarrow{W}) \tag{52}$$

$$dis(f) = dis(Cir) + dis(Lin) \tag{53}$$

$$dis(f) = r_{t_{min_i}}\left(\left(1 - sgn(\chi_{\bar{X}_{i+1}} - \chi_{\bar{X}_i})\Omega_i +\right)\pi + \Omega_i(\chi_{\bar{X}_{i+1}} - \chi_{\bar{X}_i})\right) + |\bar{X}_{i+2} - \bar{X}_{i+1}| \tag{54}$$

$$dis(\overrightarrow{W}) = \overrightarrow{W} \cdot \frac{\overrightarrow{V_a}}{|\overrightarrow{V_a}|}\Delta t = \overrightarrow{W} \cdot \frac{\overrightarrow{V_a}}{|\overrightarrow{V_a}|^2} dis(f) \tag{55}$$

$$\begin{cases} i = 1,2,\dots,m \\ V_a = V_g = \sqrt{\dfrac{2F_w}{\rho S\sqrt{{C_L}^2 + {C_D}^2}}} \\ \dot{\lambda} = \dfrac{(\dot{w} + \dot{W}_z)}{(u + W_x)(1 + \tan^2\lambda)} \\ r_{t_{min}} = \dfrac{\dot{\chi}}{\left(V_g + \overrightarrow{W} \cdot \dfrac{\overrightarrow{V_a}}{|\overrightarrow{V_a}|}\right)\cos\gamma} \\ \Omega = \hat{e}_\theta \end{cases} \tag{56}$$

Equations (51) to (55) denote the effect of wind on cost function g concerning the main states X based on governing Eqs. (56) as dynamic constraints. Penalty function can also be defined to ensure obstacle avoidance according to the location of obstacles (X_{obs}) and the correct placement of the aircraft at the proper altitude at the beginning of the runway as Eqs. (57) and (58).

$$P_1 = \sum_{i=1}^{m} \frac{1}{(\bar{X}_i - X_{obs})^2} \tag{57}$$

$$P_2 = \left(z_f - z_{runway}\right)^2 \tag{58}$$

The steps of Dubins in the inner layer of minimization and proposed Hybrid Dubins-SA (HDSA) are represented as the following pseudo-codes:

Algorithm1: Inner Loop Dubins Minimization

01. ***For*** *candidate middle Turns* ***to*** *complete space*
02. ***Call*** *outer Optimization Loop*
03. ***Input****: middle Turns (*$m, r_{t_{min}}\ \bar{X}_{dis}$*)*
04. ***Sort (***$r_{t_{min}}\ \bar{X}_{dis}$***)***
05. ***Solve (****a,b,c,d as tangent point****)***
06.
$$\begin{cases} \boldsymbol{d}-\boldsymbol{b}=\boldsymbol{s}(\boldsymbol{c}-\boldsymbol{a}) \\ \boldsymbol{b}-y_0=-\frac{1}{\boldsymbol{s}}(\boldsymbol{a}-x_0) \\ \boldsymbol{d}-y_1=-\frac{1}{\boldsymbol{s}}(\boldsymbol{c}-x_1) \\ (\boldsymbol{a}-x_0)^2+(\boldsymbol{b}-y_0)^2={r_0}^2 \\ (\boldsymbol{c}-x_1)^2+(\boldsymbol{d}-y_1)^2={r_1}^2 \end{cases}$$
07. ***Distance(***$r_{t_{min}}, a, b, c, d$***)***
08. ***Min(Distance):*** 2^{n+2}*trajectories for n middle turns*
09. ***Goto*** *02*
10. ***End-For***

Algorithm2: Dubins-SA Engine

01. ***Input****:* $m, N_{\bar{X}_{dis}}, \alpha, T_{initial}$
02. ***while (***$T > T_{terminal}$***)***
03.control point: $m, \bar{X}_{dis}, r_{t_{min}}$;
04.count=1;
05. ***while*** $(count < Threshold)$
06.Tr=Dubins ($m, \bar{X}_{dis}, r_{t_{min}}$*)*
07. ***Generate*** *3D Tr=Tr(*$m, \bar{X}_{dis}, r_{t_{min}}, V, \gamma$*)*
08.old cost = calculate obj(G*)*
09. ***select****(control point)*
10.new cost = calculate obj(G*);*
11. ***if*** *(isAccept(old cost, new cost))*
12. ***update*** *control point;*
13.old cost = new cost;
14. ***if*** *check(terminate condition not met)*
15. ***Goto*** *06*
16. ***else****;*
17. ***Break***
18. ***End-if***
19.count=count+1;
20. ***End-while***
21. ***update****Temprature(*$T = \alpha T$*);*
22. ***update*** $m, \bar{X}_{dis}, r_{t_{min}}$ *at each reduction of temperature T*
23. ***End-while***

C. Complexity Analysis

Given the real-time structure demand, some assumptions can be used to decrease the run-time of the problem to create efficient trajectories. It is possible to rewrite the optimal trajectories of Eq. (44) as follows:

$$Tr^* = min\left[G\left(\bigcup_{j=1}^{n}\left[\sum_{i=1}^{m} f_i^{\,j}\right]\right)\right] \tag{59}$$

$$Tr^* = min\left[G\left(min_j\left(\left[\sum_{i=1}^{m} f_i^{\,j}\right]\right)\right)\right] \tag{60}$$

The result of the inner minimization of Eq. (60) is due to the Dubins algorithm in each iteration remove some candidate paths and provide the minimum unique path to find the optimal location of middle points in outer minimization. In fact, due to the analytical nature of Dubins minimization, part of the complexity of the response space is removed Consequently, the following equation reduces the number of input candidate routes to the optimization algorithm from $2^{n_{MT}+4} + n_{MT}\ 2^{n_{MT}+3}$ to $2^{n_{MT}+2}$. Moreover, by discretizing the geometric location of the middle turn continuous

search space $O_{free} \subseteq O$, the solution space of the optimization algorithm is confined to limited discrete points. Accordingly, the run-time is considerably decreased as the following equations.

$$\forall \bar{X} = \begin{bmatrix} x \\ y \\ z \end{bmatrix} \subseteq O_{free}, \exists \bar{X}_{dis} = \bigcup \begin{bmatrix} x_k \\ y_k \\ z_k \end{bmatrix}; k \in \mathbb{N} \tag{61}$$

$$\begin{bmatrix} x_k \\ y_k \\ z_k \end{bmatrix} = discrete\left(\begin{bmatrix} x \\ y \\ z \end{bmatrix}\right) \tag{62}$$

If the number of members of $\bar{X}_{dis}$ is $N_{\bar{X}_{dis}}$, the maximum configuration space of total trajectories permutation for m middle turn is ${N_{\bar{X}_{dis}}}^{m}$. The HDSA algorithm would be a complete space search that searches all possible configurations until finding the minimum. The current problem would entail an exponential complexity order $O({N_{\bar{X}_{dis}}}^{m})$ in the whole searching space.

As mentioned before, SA is based on metallurgical practices by heating from an initial temperature $T_{initial}$ to a high temperature and cooled by cool rate α. It goes through $O(\log N_{\bar{X}_{dis}})$ temperature steps. For each temperature, the search examines $O(N_{\bar{X}_{dis}})$ attempted and accepted changes. Consequently, the run-time of the SA algorithm reduces the complexity of $O\left(\left({N_{\bar{X}_{dis}}}^{2} + N_{\bar{X}_{dis}}\right)\log N_{\bar{X}_{dis}}\right)$. Since most steps take place at low temperatures, where most changes are rejected, the term $O\left(N_{\bar{X}_{dis}} \log N_{\bar{X}_{dis}}\right)$ is not negligible comparing the term $O\left({N_{\bar{X}_{dis}}}^{2} \log N_{\bar{X}_{dis}}\right)$.

V. Simulations and Results

The simulations are based on post-failure trajectory planning regarding dynamic constraints $r_{t_{min}}$, Ω, V_a , and $\dot{\gamma}$ to land on the desired runway position, direction, and altitude. Therefore, trajectory generation and analysis of the middle turns are evaluated in the first section of the simulations. In the second section, trajectory planning respecting obstacle avoidance and wind field, are considered applying the HDSA optimization and dynamic constraints. Finally, two scenarios with limited turn capabilities based on real historical cases are investigated to demonstrate the effectiveness of the proposed strategy. All simulations are performed using the Airbus A320 model with an approach speed of 225 knots. The start point of the simulations is considered to be 12.43 miles (20 *km*) away from the runway located at the origin (0, 0, 0) as the final point.

A. Trajectory Generation and Middle Turns

The presented trajectory generation strategy is based on Dubins paths and Apollonius results to find the optimal trajectories, while applying middle turns to the trajectories. Figs. 8 and 9 illustrate the straight (with no middle turns) optimal trajectories for different initial headings and different runway orientations in 2D and relevant 3D views. Fig. 8 represents different values for the initial heading at the time of decision for the landing process, while Fig. 9 represents the same scenarios for different values of runway headings. Same simulations are represented in Figs. 10, 11, and 12, while applying one middle turn during the optimal trajectory design. The applications of middle turns on the trajectories are considered at fixed pre-determined positions during the simulations. As mentioned, adding middle turns causes a better route to pass obstacles, having lower crosswinds or producing more distance to reduce flight altitude. Figure 13 also illustrates the effect of middle turns on the optimized routes for pre-determined positions of one, three, five, and seven middle turns. These simulations are based on analytical mathematical solutions of tangent lines. Fig. 13 shows the effect of the route generation algorithm to produce the related trajectory based on the arbitrary number of middle turns in desired locations. The produced results show the flexible pattern of mathematical equations to produce 3D paths in straight and circular lines.

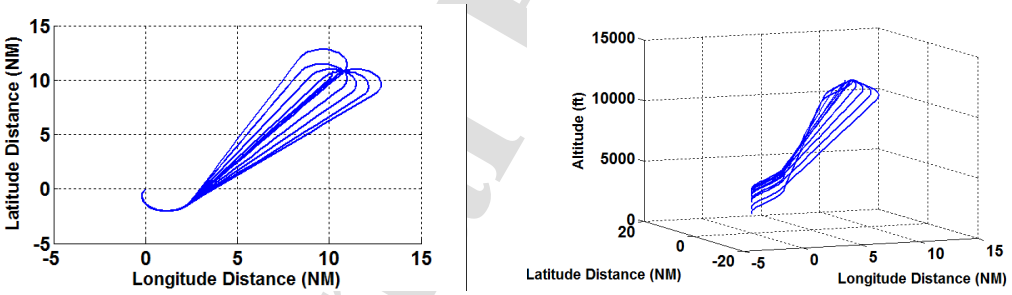

Fig. 8 Optimal direct trajectories with no middle turn for different initial headings (initial heading from 0 to 360 degrees).

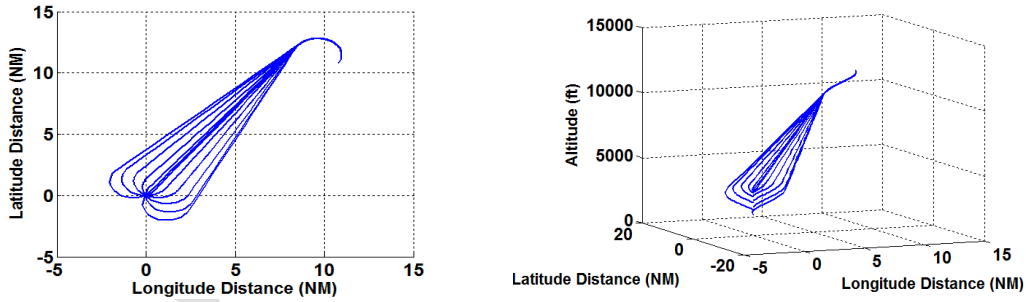

Fig. 9 Optimal direct trajectories with no middle turn for different runway orientations (runway orientations from 0 to 360 degrees).

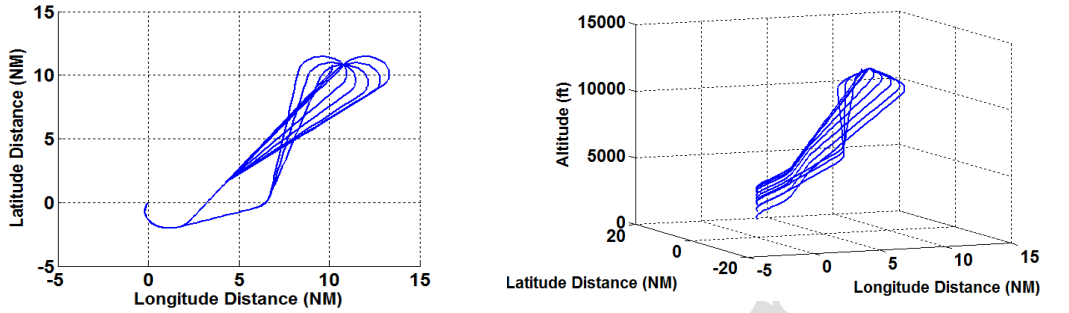

Fig. 10 Optimal trajectories with one middle-turn with different initial headings (initial heading from 0 to 360 degrees with fixed middle turn position).

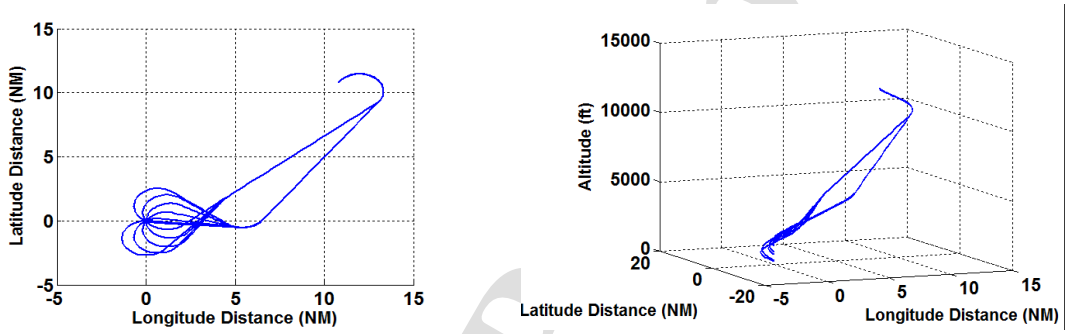

Fig. 11 Optimal trajectories with one middle turn and different runway orientations (runway orientations from 0 to 360 degrees with determined middle turn position).

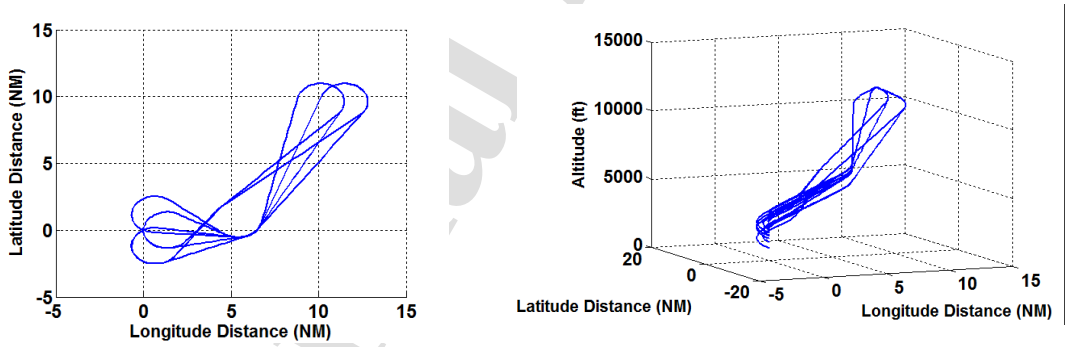

Fig. 12 Optimal trajectories with one middle turn and combinations of different initial and final headings (initial headings and runway orientations vary from 0 to 360 degrees with pre-determined fixed middle turn positions)

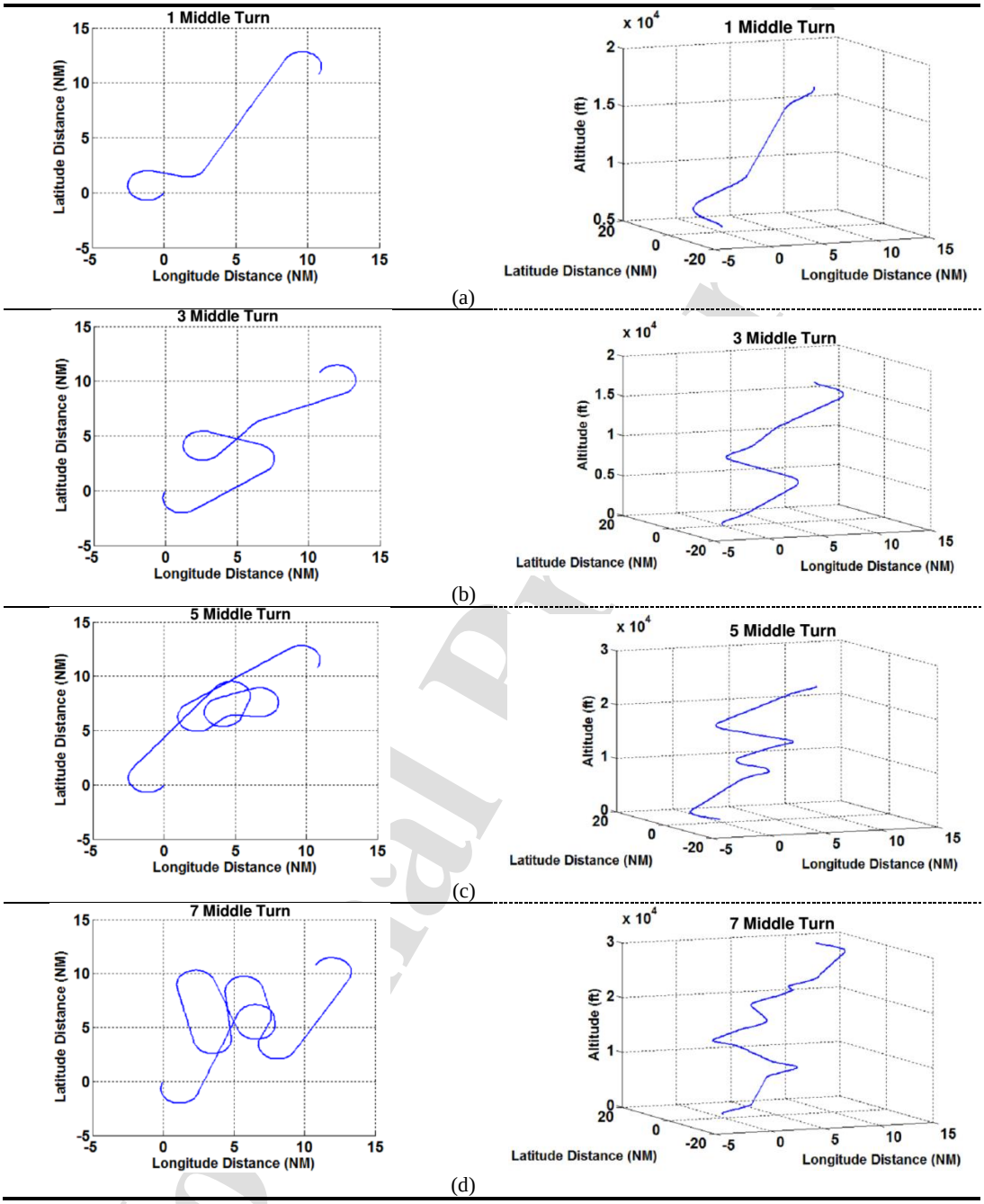

Fig. 13 Effect of middle turns, one, three, five, and seven middle turns, left: up view (2D view) of the trajectory, right: the 3D landing trajectory. a- 1 middle turn, b- 3 middle turns, c- 5 middle turn, and d- 7 middle turn

B. Wind and obstacles

The approach for obstacles avoidance and flying through the wind and environmental uncertainty is based on finding the optimal location of middle turns applying HDSA and penalty function. The optimal trajectories depend on selecting the middle turns so that the minimum crosswind is guaranteed as well as crossing the obstacles. The initial temperature of HDSA is $T_0 = 6000$, where the cooling schedule experiences the temperature increase at some points because of escaping from local minimums. The concept of discrete environment in continuous analytical solutions tends to decrease the run-time of finding the best locations [35]. Figs. 14 and 15 illustrate the flight path through different wind fields with only one and two middle turns. Two kinds of linear and non-linear (sinusoidal) wind fields are considered in the simulations. Increasing the number of middle turns will result in a smoother and more efficient flight path during the maneuver, while the run-time increases exponentially. Different scenarios of obstacle avoidance are illustrated in Fig. 16 regarding the optimal candidate trajectories in the presence of the wind.

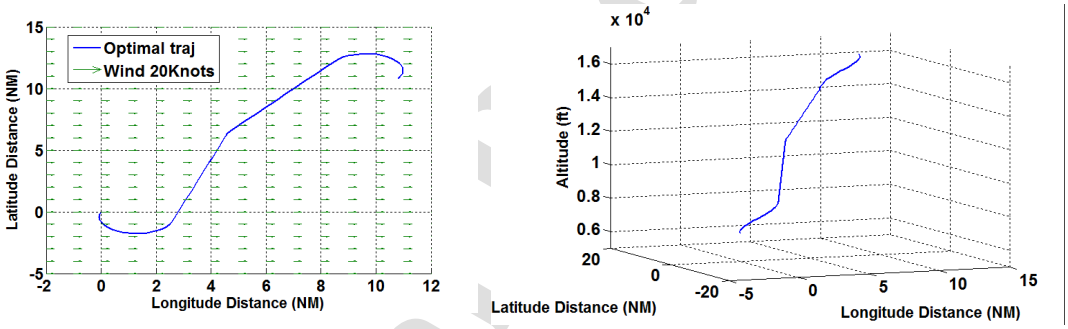

Fig. 14 One middle turn with the linear wind field effect.

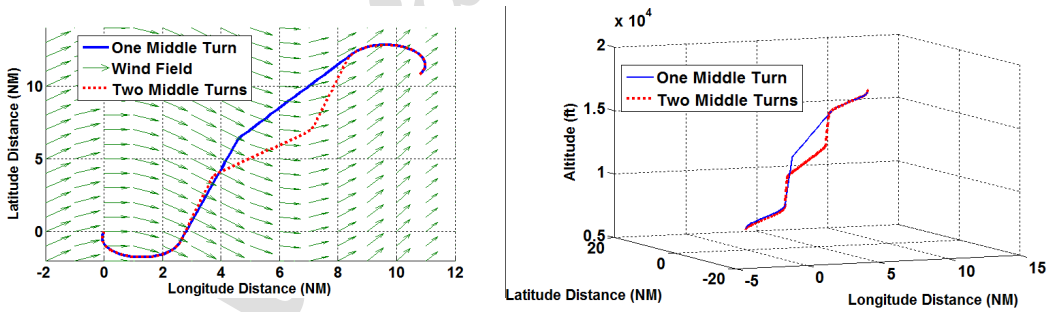

Fig. 15 Nonlinear wind field effect with one and two middle turns.

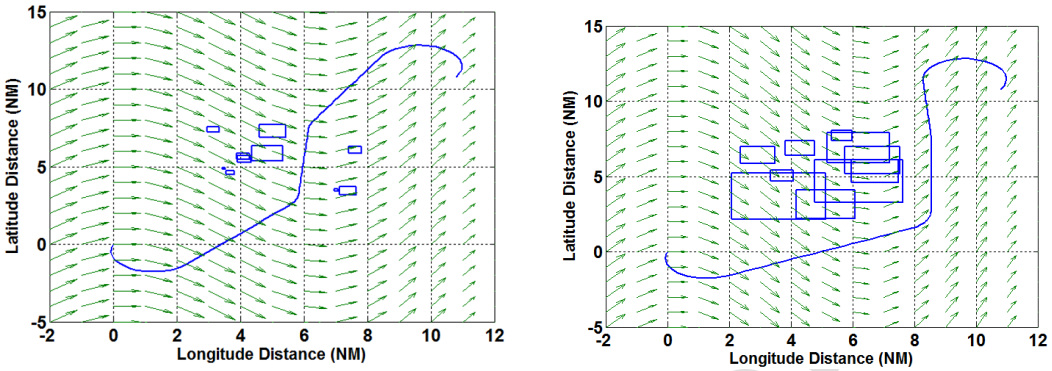

Fig. 16 Obstacle avoidance in the wind field

C. Different turn radius and limited turns

In some emergency cases following fault of failure, the aircraft performance might severely degrade and be confined to one specific direction (just turn to the right or t the left direction) of bigger turn radiuses (with less turn rates). Two scenarios of limited turn capabilities with different turn radiuses and directions are considered in this section. The optimal flight trajectories are illustrated in Fig. 18 (left and right) with different turn radiuses. Fig. 19 represents a real case of approaching the "Toulouse Blagnac" runway (TLS- 32/14 L, R), with only left turn capability with different turn radiuses. The simulations demonstrate the effectiveness of the proposed architecture in finding middle turns in different scenarios.

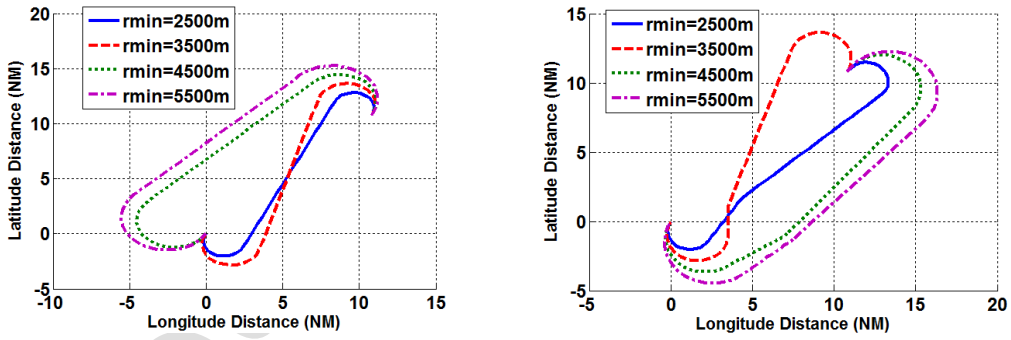

Fig. 17 Optimal trajectories with different radiuses, left: direct trajectory with no middle turn, right: trajectories with one middle turn.

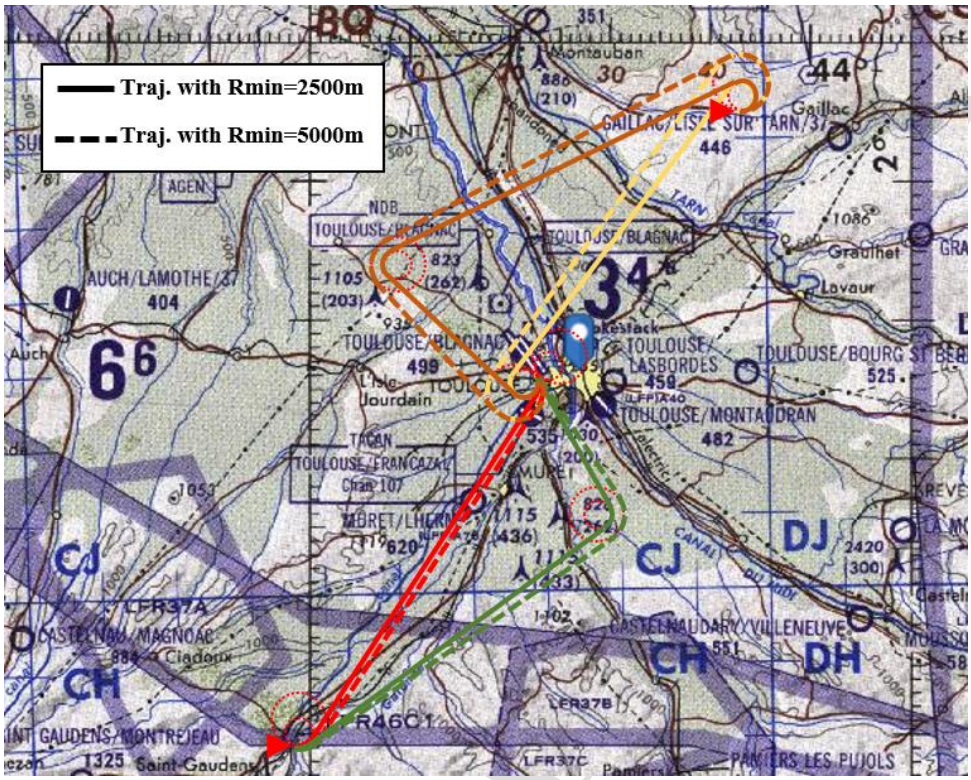

Fig. 18 Different post-failure emergency trajectories to Toulouse Blagnac runway (TLS- 32/14 L,R), only left turn is permitted with minimum turning radius 2500 meter (solid line) and 5000 meters (dashed line).

Table 6 illustrates the complexity in terms of run-time and requires time according to failure and aircraft response. All of the simulations are performed by Matlab R2019 and Linux on a computer with Intel core i7, 2.13 GHz processor, and 8 GB RAM.

Table 6. Complexity Analysis

Cases	Distance to Runway, miles	Aircraft velocity, knots	Available time, sec	HDSA Run time, sec	SA Runtime, sec
Right turn failure	50	225	695	3.667	35.432
Left turn Failure	50	225	695	3.863	41.863
Induced bank	50	200	782	3.462	33.593
Thrust failure	50	180	869	4.231	56.321

VI. Conclusion

Flight operations must be safe, efficient, and comply with air-space restrictions and air-traffic control directives. When a major aircraft system fails, safety becomes the overriding priority and the main goal is to safely land the aircraft. Regarding this objective, this work includes three main parts: 1- post-failure dynamic performance analysis, which calculates the constraints, 2- route generation pattern based on geometrical Dubins analysis and effects of middle turns, and 3- trajectory planning based on a hybrid form of Dubins and Simulated Annealing (SA). A Hybrid form of the Dubbin-SA equation (HDSA) is formulated to solve the problem of post-failure optimal landing trajectories, given an initial and final position and heading, under the airplane dynamic and performance constraints.

Emergency flight conditions can occur at any altitude, airspeed, and flight phase. The type of possible trajectories to reachable runways may vary depending on the post-failure airplane performance. Five different types of failure scenarios including lift reduction, control surface failure (induced bank angle), thrust reduction, drag reduction (landing gear failure), and engine failure (asymmetric thrust) are investigated as different types of emergency conditions. Lift reduction increases the turning radius and glide acceleration, which increases the path angle and the landing speed. Induced bank angle causes an unwanted rotation on one side and increases the turn radius on the opposite side. It also letdowns the balance of the aircraft's gravitational direction and reduces the aircraft's lift force and consequently increases the touchdown speed. Thrust reduction reduces the total velocity and radius of turn and consequently increases the gliding velocity. Drag reduction increases the total velocity, turning radius, and glide ratio. It also increases the touchdown velocity and causes a longer landing distance. Asymmetric thrust has the problems of reducing the thrust and the induced bank angle, simultaneously. It reduces the total velocity and glide ratio, while confines the turning radius.

To maximize flight plan simplicity and to minimize computational complexity, flight plans are designed to fit within the middle turns and analytical solution of Dubins routes for a group of middle turns, which are commonly used for both piloted and autonomous landing flight plans. The location of the middle turns and the optimized values of dynamic constraints are the parameters of the optimization process. Results illustrate the HDSA operation for a variety of scenarios, including several cases of middle turns, obstacle avoidance, and optimal path in the wind fields.

According to the results, geometrical analysis creates fast routes, therefore the optimization process is limited to finding key waypoints and will eventually increase the efficiency of the algorithm response. In fact, the location of waypoints represents the line equation between the aircraft and the runway orientation in path generation processing.

Considering the correct location of the middle turns has played an efficient effect on passing the crosswind and obstacles avoidance. Certainly, the inclusion of a terrain database is required to enable off-runway processing and, perhaps more fundamentally, to enable verification that post-failure trajectories do not affect terrain and buildings. More research is required to enable an aircraft to accurately and automatically generate post-failure performance models for the spectrum of failures and structural damage cases. Generally, independent of the specific failure, the trajectory generation process is integrally tied to flight envelope constraints. Work is ongoing to systematically expand the set of failures handled by the simulations, beginning with an examination of failures by high-fidelity flight simulators and Flight Data Recorder (FDR) analysis of aircraft during failure and landing. We refer the reader to a future publication for a rigorous analysis of the proposed.

References

[1] Ahmadi, K., Asadi, D., Pazooki, F., "Nonlinear L1 adaptive control of an airplane with structural damage," *Proceedings of the Institution of Mechanical Engineers, Part G: Journal of Aerospace Engineering*, Vol. 233, No. 1, 2017, pp. 341-353. doi: 10.1177/0954410017730088

[2] Asadi, D., Atkins E. M., "Multi-Objective Weight Optimization for Trajectory Planning of an Airplane with Structural Damage," *Journal of Intelligent & Robotic Systems*, Vol. 91, No. 3-4, 2018, pp. 667-690. doi: 10.1007/s10846-017-0753-9.

[3] Donato, D., Pedro, F.A., Atkins, E. M., "Evaluating risk to people and property for aircraft emergency landing planning," *Journal of Aerospace Information Systems*, Vol. 14, No. 5, 2017, pp. 259-278. doi: 10.2514/1.I010513.

[4] Asadi, D., Sabzehparvar M., Atkins, E. M., Talebi, A., "Damaged airplane trajectory planning based on flight envelope and motion primitives," *Journal of Aircraft*, Vol. 51, No. 6, 2014, pp. 1740-1757. doi: 10.2514/1.C032422.

[5] Asadi, D., Sabzehparvar, M., and Talebi, H., A., "Damaged airplane flight envelope and stability evaluation," *Aircraft Engineering and Aerospace Technology*, Vol. 85, No. 3, 2013, pp. 186-198. doi: 10.1108/00022661311313623.

[6] Asadi D, Ahmadi K., "Nonlinear robust adaptive control of an airplane with structural damage," *Proceedings of the Institution of Mechanical Engineers, Part G: Journal of Aerospace Engineering*, Vol. 234, No. 14, 2020, pp. 2076-2088. doi:10.1177/0954410020926618.

[7] Asadi D, Bagherzadeh S., "Nonlinear adaptive sliding mode tracking control of an airplane with wing damage," *Proceedings of the Institution of Mechanical Engineers, Part G: Journal of Aerospace Engineering*, Vol. 232, No. 8, 2018, pp. 1405-1420. doi:10.1177/0954410017690546.

[8] D. Asadi, "Partial engine fault detection and control of a Quadrotor considering model uncertainty," *Turkish Journal of Engineering*, Vol. 6, No. 2, Apr. 2022, pp. 106-117.
doi:10.31127/tuje.843607.

[9] Calise, A., J., and Rysdyk. R., T., "Nonlinear adaptive flight control using neural networks," *IEEE Control Systems Magazine*, Vol. 18, No. 6, 1998, pp. 14-25.
doi: 10.1109/37.736008.

[10] Kumar, D., N., Verma, N., K., and Behera, L., "Adaptive critic-based event-triggered control for HVAC system," *IEEE Transactions on Industrial Informatics*, Vol. 14, No. 1, 2017, pp. 178-188.
doi: 10.1109/TII.2017.2725899.

[11] Gundy-Burlet, K., Krishnakumar, K., Limes, G., and Bryant, D., "Augmentation of an intelligent flight control system for a simulated C-17 aircraft," *Journal of Aerospace Computing, Information, and Communication*, Vol. 1, No. 12, 2004, pp. 526-542.
doi: 10.2514/1.13246.

[12] Asadi, D., Ahmadi, K. & Nabavi, S.Y., *Fault-tolerant Trajectory Tracking Control of a Quadcopter in Presence of a Motor Fault*, Int. J. Aeronaut. Space Sci, 2021.
doi: https://doi.org/10.1007/s42405-021-00412-9.

[13] Mettler, B., Valenti, M., Schouwenaars, T., Kuwata, Y., How, J., Paunicka, J., & Feron, E., "*Autonomous UAV guidance build-up: Flight-test demonstration and evaluation plan,"* AIAA Guidance, Navigation, and Control Conference and Exhibit, 2003, pp. 5744.
doi: 10.2514/6.2003-5744.

[14] Haghighi, H., Sadati, S. H., Karimi, J., & Dehghan, M. M., "A Hierarchical and Prioritized Framework in Coordinated Maneuver of Multiple UAVs Based on Guidance Regulator," *Journal of Aerospace Technology and Management*, Vol. 11, No.1, 2019.
doi: 10.5028/jatm.v11.999.

[15] Boskovic, J., Prasanth, D., R., and Mehra, R., K., "A multi-layer autonomous intelligent control architecture for unmanned aerial vehicles," *Journal of Aerospace Computing, Information, and Communication*, Vol. 1, No. 12, 2004, pp. 605-628.
doi: 10.2514/1.12823.

[16] Boskovic, J., and Mehra. R., *"An Integrated Fault Management System for Unmanned Aerial Vehicles,"* 2nd AIAA Unmanned Unlimited Conf. and Workshop & Exhibit, 2003, pp. 6642.
doi: 10.2514/6.2003-6642.

[17] Steven Q., Ludkovski, M., and Hespanha, J., P., "Stochastic optimal coordination of small UAVs for target tracking using regression-based dynamic programming," *Journal of Intelligent & Robotic Systems*, Vol. 82, No. 1, 2016, pp. 135-162.
doi: 10.1007/s10846-015-0270-7.

[18] Schouwenaars, T., Mettler, B., Feron, E., and How, J. P., *"Robust motion planning using a maneuver automation with built-in uncertainties."* Proceedings of the 2003 American Control Conference, IEEE, Vol. 3, 2003, pp. 2211-2216. (2003, June).
doi: 10.1109/ACC.2003.1243402.

[19] Yi, G. and Atkins, E., M., *"Trim state discovery for an adaptive flight planner,"* paper presented at AIAA Guidance Navigation and Control Conference Orlando, FL, USA, available at: deepblue.lib.umich.edu/bit stream/ 2027/AIAA-2010-416-783.
doi: 10.2514/6.2010-416 .

[20] Valenti, M., Mettler, B., Schouwenaars, T., Feron, E., and Paduano, J., *"Trajectory reconfiguration for an unmanned aircraft,"* AIAA Guidance, Navigation, and Control Conference and Exhibit. 2002 pp. 4674.
doi: 10.2514/6.2002-4674.

[21] Dubins, L., E., "On curves of minimal length with a constraint on average curvature, and with prescribed initial and terminal positions and tangents," *American Journal of mathematics*, Vol. 79, No. 3, 1957, pp. 497-516.
doi: 10.2307/2372560.

[22] Jérôme, B., and Latombe, J., C., "Nonholonomic multibody mobile robots: Controllability and motion planning in the presence of obstacles," *Algorithmica*, Vol. 10, No. 2-4, 1993, pp. 121.
doi: 10.1007/BF01891837.

[23] Pankaj K., A., Raghavan, P., and Tamaki. H., *"Motion planning for a steering-constrained robot through moderate obstacles,"* Proceedings of the twenty-seventh annual ACM symposium on Theory of computing, 1995, pp. 343-352.
doi: 10.1145/225058.225158.

[24] Ryo, T., and Tsai, R., "Optimal trajectories of curvature constrained motion in the Hamilton–Jacobi formulation," *Journal of Scientific Computing*, Vol. 54, No. 2-3, 2013, pp. 622-644.
doi: 10.1007/s10915-012-9671-y.

[25] Atkins, E. M., Portillo, I. A., and Strube, M. J., "Emergency flight planning applied to total loss of thrust," *Journal of aircraft*, Vol. 43, No. 4, 2006, pp. 1205-1216.
doi: 10.2514/1.18816.

[26] Timothy, M., Beard, R., W., and Owen, M., *"Implementing Dubins airplane paths on fixed-wing UAVs,"* 1677–1701. Springer Link, Netherlands, 2014, pp. 1677-1701.

[27] Arno, F., and Messnarz. B., "Automated trajectory generation and airport selection for an emergency landing procedure of a CS23 aircraft," *CEAS Aeronautical Journal*, Vol. 8, No. 3, 2017, pp. 481-492.
doi: 10.1007/s13272-017-0252-5.

[28] Haghighi, H., Asadi, D., Delahaye, D.; 'Multi-Objective Cooperated Path Planning of Multiple Unmanned Aerial Vehicles Based on Revisit Time', *Journal of Aerospace Information Systems, 1-14*, 2021.
doi: 10.2514/1.I010866.

[29] Haghighi, Hassan, Sadati, S. H., Dehghan, S. M., & Karimi, J.; "Hybrid Form of Particle Swarm Optimization and Genetic Algorithm For Optimal Path Planning in Coverage Mission by Cooperated Unmanned Aerial Vehicles". *Journal of Aerospace Technology and Management*, 2020, 12.
doi: 10.5028/jatm.v12.1169.

[30] Yang, L., Qi, J., Song, D., Xiao, J., Han, J., and Xia, Y., "Survey of robot 3D path planning algorithms," *Journal of Control Science and Engineering*, Vol. 1, No. 1, 2016.
doi: 10.1155/2016/7426913.

[31] Coxeter, H. S. M., "The problem of Apollonius," *The American Mathematical Monthly*, Vol. 75, No. 1, 1968, pp. 5-15.
doi: 10.1080/00029890.1968.11970941.

[32] Laarhoven, V., Peter J., M., and Aarts. E., *"Simulated annealing: Theory and applications,"* Springer, Dordrecht, 1987, pp. 7-15, Print ISBN: 978-90-481-8438-5.

[33] Delahaye, D., Supatcha C., and Marcel, M., *"Simulated annealing: From basics to applications,"* Handbook of Metaheuristics. Springer, Cham, (ISOR, volume 272) 2019. 1-35.

[34] Courchelle, V., Delahaye, D., González-Arribas, D., and Soler, M., "Simulated Annealing for Strategic Traffic De-confliction by Subliminal Speed Control under Wind Uncertainties," *HAL archives, hal-enac.archives-ouvertes.fr*, 2017.

[35] Hassan, H., Heidari, H., Sadati, S. H., & Karimi, J.; "*A hierarchical and priority-based strategy for trajectory tracking in UAV formation flight"*; 8th International Conference on Mechanical and Aerospace Engineering (ICMAE), pp. 797-800; IEEE, 2017.
doi: 10.1109/ICMAE.2017.8038752.

- A hybrid form of Dubins and a meta-meuristic optimization algorithm
- The post-failure performance characteristics of the distressed airplane is applied.
- Route generation and optimization strategies
- Analytical performance-based equations to achieve an optimal trajectory planning.
- A fast and safe emergency landing trajectory in presence of obstacles.
- To maximize flight plan simplicity and to minimize computational complexity
- Dubins routes are used for middle turns in autonomous landing flight plans.
- Simulated annealing is used to select the optimal combination of the candidate trajectories.

Hassan Haghighi: Conceptualization, Methodology, Software, Writing- Original draft preparation.

Daniel Delahaye.: Data curation, Editing the Draft, Supervision, Validation.

Davood Asadi: Conceptualization, Reviewing and Editing, Validation.

Davood Asadi
Assistant Professor
Adana Alparslan turkes science and technology university, Turkey

10/10/2020

Dear Professor Mario Köppen

I wish to submit an original research article entitled "Performance-Based Emergency Landing Trajectory Planning Applying Meta-Heuristic and Dubins Paths" for consideration by Journal of Applied Soft Computing. I confirm that this work is original and has not been published elsewhere, nor is it currently under consideration for publication elsewhere and there is no conflict of interest.

Thank you for your consideration of this manuscript.

Sincerely,

Davood Asadi, Adana Alparslan Turkes science and Technology University, Aerospace Engineering Faculty, Adana, Turkey